Chemical Engineering Journal 372 (2019) 65–73

Contents lists available at ScienceDirect

Chemical Engineering Journal

journal homepage: www.elsevier.com/locate/cej

Biomass derived porous carbon for efficient capture of carbon dioxide, organic contaminants and volatile iodine with exceptionally high uptake

Hanxue Sun[a], Boli Yang[b], An Li[a,*]

[a] Department of Chemical Engineering, College of Petrochemical Engineering, Lanzhou University of Technology, Lanzhou 730050, PR China
[b] CCDC Changqing Downhole Technology Company, Xi'an 710018, PR China

HIGHLIGHTS

- Biomass derived porous carbon from spongy flesh of sunflowers was prepared.
- The porous carbon has high surface area (up to 3072 $m^2 g^{-1}$) and light bulk density.
- The resulting porous carbon exhibits outstanding iodine uptake of 646 wt%.

ARTICLE INFO

Keywords:
Porous carbon
Sunflowers
Iodine capture
Biomass

ABSTRACT

Environmentally sustainable development and concerns have increased interested in biomass materials for synthesis of porous carbons, especially as effectively alternative and multifunctional sorbents for diverse contaminates and in CO_2 adsorption area. In this work, spongy flesh from receptacle and stalk of sunflowers was utilized as carbonaceous precursors to prepare porous carbons by pyrolysis method with and without KOH activation in argon. The biomass-derived porous carbon has high surface area (up to 3072 $m^2 g^{-1}$), light bulk density (0.033 $g cm^{-3}$) and different morphology depending on the preparation method. Taking advantages of the highly porosity and the valuable hierarchical porous structure, the resulting porous carbons can serve well as multifunctional solid sorbents for CO_2, radioactive iodine and oily/organic contaminates from water. In particular, the resulting carbon sample shows a high iodine affinity with an uptake of 646 wt%, which is the highest value reported to date. Given the worldwide abundance and recyclability, spongy flesh from receptacle and stalk of sunflowers can be serve as a new biomass source for the facile production of high-performance porous carbon materials with promising applications in environmental remediation.

1. Introduction

Carbonaceous materials are ubiquitous in various technological applications and constitute an extensive research area that has attracted considerable attention for separation media [1], energy generation and storage [2], water purification [3,4] and heterogeneous catalysis [5] etc., because of theirs numerous exceptional characteristics. In particular, porous carbon materials enjoys a place of pride as solid sorbents for gas storage and water purification mainly due to their wide precursor sources, highly developed porosity, moderate cost, high tolerance and environmentally benign nature [6]. To date, a great number of porous carbon sorbents with different architectures, porosities and morphology have been designed and developed. For example, Wilcox et al. synthesized porous carbons from 3D hierarchical nanostructured polymer hydrogels with an optimized surface area of up to 4196 $m^2 g^{-1}$ [7]. Yu et al. reported a type of carbon nanofiber aerogel [8]. Ling et al. synthesized a hierarchical carbon nanosheet-based network using graphene oxide as the structure-directing agent [9]. All these porous carbon materials as efficient sorbents exhibit good capacity for gas or harmful components.

Generally speaking, the synthesis approaches and carbonaceous sources are two crucial issues for the development of carbon sorbents with a well-developed porous structures. As is generally organized, there are two direct process to synthesize porous carbon sorbents. The first one is based on a physical activation approach, in which the system is fabricated by gasification of the carbonaceous sources in the presence of CO_2 or steam [10]. This approach imparts well-developed carbon structures with a higher degree of graphitization accompanied by lower carbon yield because of the removal of a large amount of internal carbon during activation [11]. The alternative to the physical activation

* Corresponding author.
E-mail address: lian2010@lut.cn (A. Li).

https://doi.org/10.1016/j.cej.2019.04.061
Received 12 January 2019; Received in revised form 22 March 2019; Accepted 9 April 2019
Available online 10 April 2019
1385-8947/

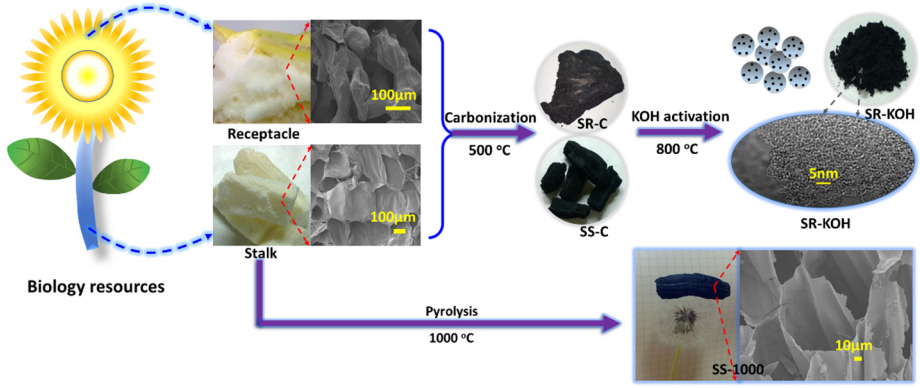

Scheme 1. The fabrication of porous carbons from the spongy flesh in the receptacle and in the centre of stalk.

described above is chemical activation. In the case of chemical activation process, the carbonaceous precursors would react with chemical agents such as KOH and the carbon atoms were etched to generate hierarchical porous microstructure [11–13]. This approach takes some several advantages of lower activation temperature, shorter heat treatment times and higher carbon yield [11], which has been regarded as an efficient way to remarkably improve the porous structures of the resulting carbon materials.

The selection of the precursor is also crucial for the final architectures and porous texture of the carbon sorbents. A great deal of carbonaceous materials including coal, poly (ionic liquid), metal organic frameworks, polymers etc. has been used for the production of porous carbon sorbents [14–16]. Among these, the preparation of porous carbon sorbents from biomass or biologically renewable resources has been approved as a sustainable approach and takes economic and application advantages. A great deal of work has successfully converted the biomass or biologically renewable resources into porous carbon sorbents through various methods [17–20]. Huang and Liu et al. prepared glucose- and chitosan-based porous carbons with ultrahigh pore volume for selective capture of CO_2 [20,21]. Wang et al. used the waste celtuce leaves to prepare porous carbon with excellent CO_2 adsorption capacity at ambient pressure [17]. Feng et al. synthesized porous carbon spheres by a simple carbonization of the fruit of Liqudambar formosana, which exhibited promising potentials for the application of oil or organic solvent spill clean-up [18]. Compared with synthetic or geological carbon resources, such strategy for preparation of porous carbon sorbents from biomass or biologically renewable resources not only reduces the fabrication cost but also promotes the utilization of biological resources in a more sustainable manner [22].

Sunflower, *Helianthus annuus L.* in Heliotropic, is one of the most important oil crops in the world. In the receptacle and stalk of sunflowers, the spongy flesh plays an important role of water storage and nutrients transport, whereas they are usually discarded or burning after the seeds used for cooking oil. Thus, the potential applications of the spongy flesh in sunflowers may has been overlooked [23]. In this paper, we focuses on recycling the spongy flesh from receptacle and stalk of sunflowers to prepare porous carbons. The porous carbons were synthesized using KOH activation and pyrolysis method. The morphology and structure as well as chemical constitution of the resulting porous carbon were characterized by Scanning electron microscopy (SEM), Transmission electron microscopy (TEM), Raman, Fourier transform infrared spectra (FTIR), elemental analysis and N_2 adsorption/desroption, in which the effect of the treatment approach on the morphology and porous texture was also illustrated. By virtual of the high surface area (up to 3072 $m^2 g^{-1}$) and availability, The resulting porous carbons shows great potentials as functional sorbents for CO_2 storage, radioactive element and organic contaminates from water. To the best of our knowledge, a feasible study of the preparing porous carbons derived from the spongy flesh of sunflowers as solid sorbents has rarely been reported, which may be provide a fundamental guidance for the practical application of biologically renewable resources from sunflowers.

2. Experimental

2.1. Pre-treatment of carbon precursors

The milky and spongy flesh from receptacle and stalk of sunflowers were collected and dried using freeze-drying method to keep its porous nature and to avoid oxidation in air. The dried flesh from receptacle was named as SR and the obtained flesh from stalk was named as SS.

2.2. Preparation of porous carbons

The synthesis of porous carbon involved carbonization and chemical activation. During the carbonization, the SR and SS was pulverized and heated to 500 °C under argon atmosphere with a heating rate of 2.5 °C min^{-1} and kept for 2 h. After cooling to room temperature, the sample was washed by ethanol and distilled water for several times followed by drying at 100 °C for overnight. The carbonized sample from flesh of sunflower receptacle and stalk was denoted as SR-C and SS-C, respectively. After drying, the mixture of SR-C (SS-C) and KOH power with a mass ratio of 1:5were fully physically grinded and mixed. The chemical activation was performed by heating the physical mixture under argon atmosphere. The mixture was placed in the centre of a tube furnace and then was heated to 800 °C under argon atmosphere with a heating rate of 2.5 °C min^{-1} and kept for 2 h. After cooling to room temperature, the sample was grinded and washed using aqueous HCl (0.1 mol L^{-1}, 100 mL) and then by sufficient distilled water followed by drying at 100 °C for overnight. The activated sample from SR and SS was denoted as SR-KOH and SS-KOH, respectively. To investigate the effect of preparation method on porous carbons, the SS were heated to 1000 °C under argon atmosphere with a heating rate of 2.5 °C min^{-1} and maintained for 1 h. After cooling to room temperature, the sample was washed by ethanol and distilled water for several times followed by drying at 100 °C for overnight. The carbonized flesh from SS was named as SS-1000. The preparation process is illustrated in Scheme 1.

2.3. Characterization

Raman spectrum was recorded using a micro-Ramam spectroscopy (JY-HR800, Jobin Yvon) with the excitation wavelength at 532 nm. The infrared spectra (FTIR) were recorded from 400 to 4000 cm^{-1} on a Nicolet FT-IR 360 spectrometer. Scanning electron microscopy (SEM) was performed on a field emission scanning electron microscope (JSM-6701F, JEOL) after coating the samples with Au film. Transmission electron microscopy (TEM) image was performed on a FEI (Tecnai G2 TF20) microscope. Elemental analyse was carried out on an Elementar Vario EL cube analyzer. The specific surface area was investigated using

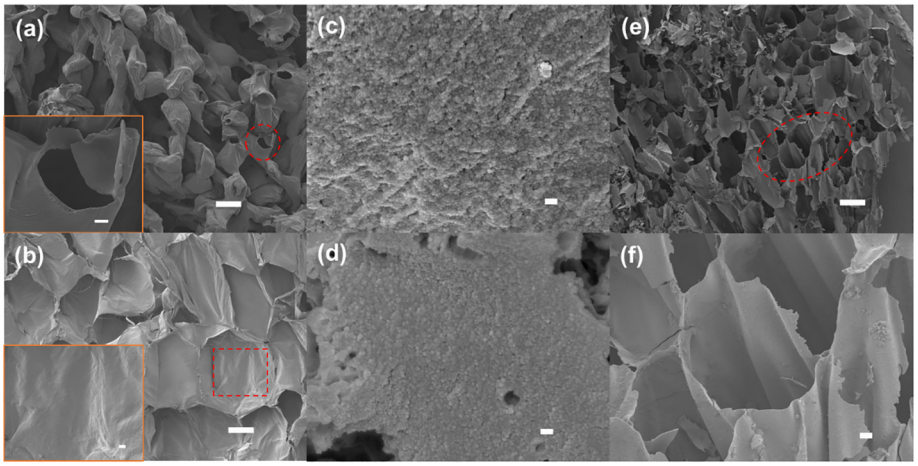

Fig. 1. SEM images of SR (a), SS (b), SR-KOH (c), SS-KOH (d) and SS-1000 (e and f). Scale bar: (a,b and e) 100 µm, (c and d) 100 nm, (a inset, b inset and f) 10 µm.

a Micrometrics ASAP 2020 system using nitrogen as the adsorbate. The CO_2 adsorption/desorption isotherms of carbon samples were measured using a Quantachrome Autosorb-1 volumetric adsorption analyzer at 0 °C and 25 °C. Before N_2 and CO_2 measurement, the sample was degassed for 12 h at 120 °C and below 1×10^{-3} mbar. Water contact angle (CA) measurement was performed on a contact angle meter OCA20 (Dataphysics, Germany). UV/Vis spectrum was recorded on a spectrophotometer (UV-2800, Unico) with the wavelength range 190–700 nm, using cyclohexane as a blank. XPS analysis was performed on a spectrometer (PHI-5300ESCA, Perkin-Elmer).

3. Results and discussion

3.1. Fabrication and structure characterizations

The milky and spongy flesh (Scheme 1), a kind of soft and porous material in the receptacle and in the centre of stalk (also named as pith), was used as the carbon precursors. The flesh from receptacle (SR) exhibits a corrected casing-liked morphology (Fig. 1a and Fig. S1a) and the sunflower pith (SS) has a connected flake morphology (Fig. 1b and Fig. S1b), both of which formed the channel for the conduction of nutrient. From the higher resolution, SR and SS show smooth and film-liked exteriors (Fig. 1a and b inset). Elemental analysis revealed that the SR contains 40.3 wt% C, 5.3 wt% H, 53.9 wt% O and 0.5 wt% N, and the SS has 32.1 wt% C, 4.6 wt% H, 62.3 wt% O and 1.0 wt% N (Table S1). For synthesis of porous carbons, we used the KOH activation, which was regards as a simple and efficient way for engineering porous structures of carbon materials. The chemical activation mainly involves reaction occurring between the carbon materials and chemical agents. During this process, the carbon framework of carbon precursors is etched by KOH to generate micro/naon pores compared with the defect-free smooth surface of SS and SR [11,12]. From the SEM images, both SR-KOH and SS-KOH show irregular and monolithic morphology (Fig. S1c and d) with nano-sized carbon particles (grain sizes ca. 20 nm) to yield a hierarchical porosity (Fig. 1c and d). XPS spectra shows that all of the resulting carbon samples mainly consists of C and O (Fig. S2). Elemental analysis exhibited that the carbon-oxygen ratio in samples greatly increased to 15.5 and 25.2 for SR-KOH and SS-KOH (Table S1). The treating method has an important effect on the morphology of the resulting carbon samples. After pyrolysis at 1000 °C, the SS-1000 kept a monolithic appearance (Scheme 1). Although the carbon content SS-1000 was increased to 77% (Table S1), SS-1000 retained the similar morphology with SS (Fig. 1e). On the other hand, the high-temperature carbonization promoted the evolution of CO_2 or CO originated from the decomposition of the small molecular organic matter, as a result, a cross-linked and macroporous structure with expanding channel was observed in SS-1000 (Fig. 1f). The bulk density were measured as 33 mg mL^{-1} for SR-KOH, SH-KOH for 80 mg mL^{-1} and 56 mg mL^{-1} for SS-1000, lower than most commercial activated carbons, which results from the unique porous structures of the samples (Fig. 1).

The typical TEM images with different magnifications were adopted to give further evidence of the morphology and structure for these carbon samples. Both SR-KOH and SS-KOH exhibited hierarchical porous texture (Fig. 2a and c). At high-magnification, the carbon skeletons of SR-KOH and SS-KOH were homogeneous and consisted of wormhole-like micro- or nanopores with no detectable larger pores (Fig. 2b and d). All carbon samples show typical amorphous structure with an amount of defects in carbon matrix. Whereas, SS-1000 was

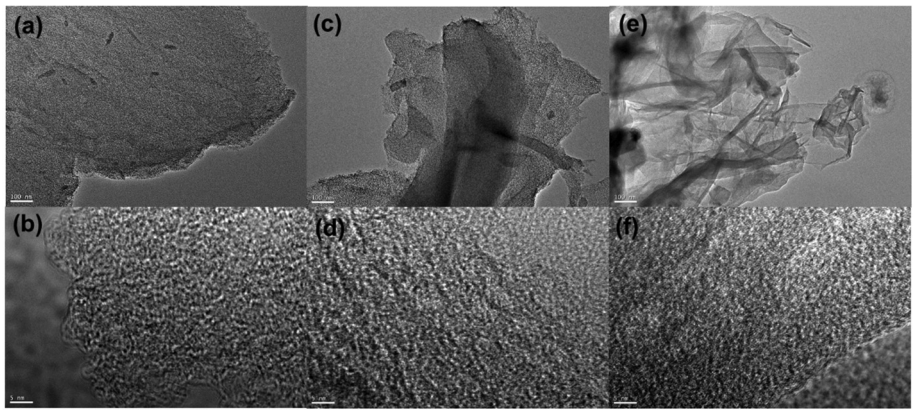

Fig. 2. TEM images of SR-KOH (a and b), SS-KOH (c and d) and SS-1000 (e and f). Scale bar: (a,b and e) 100 nm, (c,d and f) 5 nm.

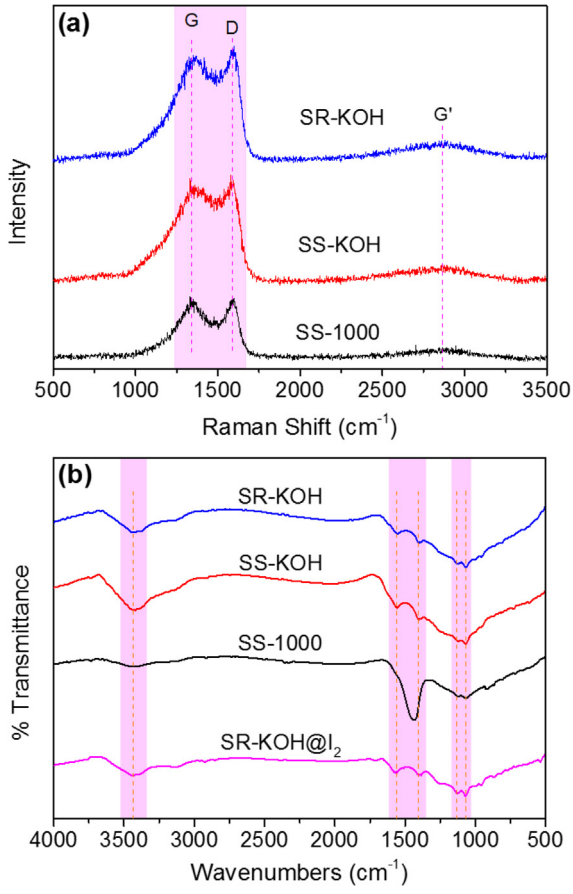

Fig. 3. (a) Raman spectra of SR-KOH, SS-KOH and SS-1000. (b) FTIR spectra of SR-KOH, SS-KOH, SS-1000 and SR-KOH@I_2.

translucent and membranous morphology (Fig. 2e) with apparent oriented multilayer domains (Fig. 2f), accordance with the SEM images. For SR-KOH and SS-KOH, however, more disordered graphene layer domains were observed compared with SS-1000, verifying that KOH activation could be more favorable to the formation of micro- or mesopores that may be beneficial for gas storage [11].

Raman spectroscopy can be used to characterize the structure of the carbon samples. As shown in Fig. 3a, all carbon samples exhibit two broad and overlapping peaks with intensity maxima at around 1590 cm^{-1} (G-band) and 1342 cm^{-1} (D-band) in Raman spectra. And the broad Raman feature appearing in the range of 2500–2800 cm^{-1} corresponds to the G'-band emphasizing a Raman-allowed mode for sp^2 carbons. The D-band peak demonstrates the existence of the disordered sections and defects in the carbon matrix. Raman spectra suggested that all carbon samples can be interpreted as disordered graphitic structures and confirmed the disordered nature of the carbons [24], accordance with TEM observation. These defects in samples are of great importance for improving the performance of porous carbons for practical applications [6]. FTIR spectroscopy was used to evaluate the surface chemistry of these carbon materials (Fig. 3b). All the resulting carbon samples exhibit adsorption bands at 3430 cm^{-1}, 1560 cm^{-1}, 1408 cm^{-1}, 1123 cm^{-1} and 1065 cm^{-1}, corresponding to the stretching vibration of −OH from the surface of carbon samples or water molecules, stretching vibration of C=C from carbon rings, the in-plane bending vibration of −OH, asymmetric stretching vibration C−O−C and stretching vibration of C−O from alcoholic and phenolic groups or bridge bonds [13]. The FTIR spectra suggests the existence of oxygen-containing groups on the surfaces of the carbon products, which was also confirmed by elemental analysis (Table S1).

In conjunction with TEM images, to evaluate the porous features of the carbon materials, nitrogen gas adsorption/desorption measurements were performed (Fig. 4a). The results are also summarised in Table 1. The nitrogen sorption isotherms for SR-KOH, SS-KOH and SS-1000 are mixed type-I and -IV with well-defined plateaus, corresponding to the filling of micropores [25]. Moreover, the broadening of the knee in the relatively low pressure range ($P/P_0 < 0.4$) for these carbon samples suggested the formation of mesopores during the activation [11,26,27]. The pore size distribution curves also confirmed the existence of both micropores and mesopores in the three carbon samples (Fig. 4b and c). The percentage of micropore volume in total pore volume was 44% and 60% for SR-KOH and SS-KOH, lower than that of SS-1000, as the result of the widening of the pre-existing micropores to mesopores [28]. The micropore sizes analysed by the Saito-Foley (SF) method of SR-KOH, SS-KOH and SS-1000 are centred at about 1.02 nm, 0.58 nm and 0.46 nm, respectively. The BET surface areas of SR-KOH, SS-KOH and SS-1000 were calculated to 3072 $m^2\ g^{-1}$, 2730 $m^2\ g^{-1}$ and 654 $m^2\ g^{-1}$. Obviously, the chemical activation can achieve higher surface area than pyrolysis. In the chemical activation process, the prominent reaction occurring between the carbon materials (SR and SS) and KOH was described as $6KOH + C \leftrightarrow 2K + 3H_2 + 2K_2CO_3$ [11,12]. Above 400 °C, the carbon was oxidized into carbonate ions and the metallic potassium penetrates between graphitic layers. As a result, the

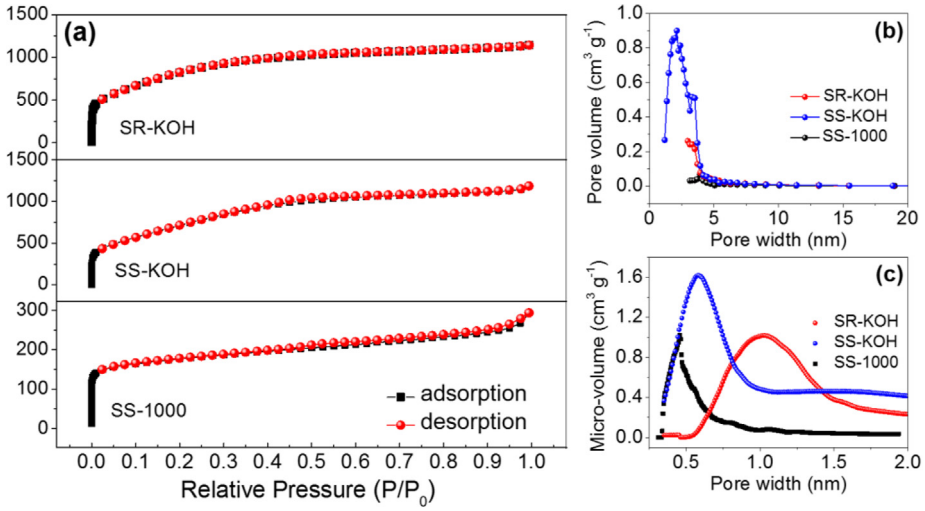

Fig. 4. (a) Nitrogen adsorption/desorption isotherms of SR-KOH, SS-KOH and SS-1000. (b) Barrett-Joyner-Halenda (BJH) desorption pore size distributions of SR-KOH, SS-KOH and SS-1000. (c) Micropore size distributions of SR-KOH, SS-KOH and SS-1000.

Table 1
Textural parameters of the carbon samples.

Samples	[a]S_{BET} (m^2 g^{-1})	[b]V_t (cm^3 g^{-1})	[c]V_{micro} (cm^3 g^{-1})	V_{micro}/V_t	[d]D_{SF} (nm)
SR-KOH	3072	1.77	0.78	44%	1.02
SS-KOH	2730	1.84	1.12	60%	0.58
SS-1000	654	0.46	0.36	79%	0.46

[a] S_{BET} is the surface area calculated using the Brunauer-Emmet-Teller (BET) method between 0.05 and 0.30 (P/P_0).
[b] V_t present the total pore volume measured at 0.995 (P/P_0).
[c] V_{micro} is micropore volume calculated using SF method.
[d] D_{SF} is the average micropore sizes calculated using SF method.

consumption of carbon, the expansion of the carbon lattice by potassium and the next removal of intercalated potassium would lead to the formation of the pore network and correspond to an increase in porosity and surface area [29].

3.2. Carbon dioxide storage

The global warming and serious climate change caused from the anthropogenic CO_2 in the atmosphere underlies the urgent need for efficient CO_2 capture and storage [30–32]. The removal of CO_2 from flue gas can be achieved using absorption materials, such as zeolites, porous polymers and carbons etc., which takes advantages of high capacity, low regeneration energy requirements and disposal/treatment costs [33,34]. Encouraged by the excellent porous properties, we investigated the CO_2 adsorption capacities of the resulting carbon materials. The adsorption isotherm measured at 273 K and 298 K by volumetric methods were shown in Fig. 5. The CO_2 uptake isotherms for these three carbon samples are entirely reversible, underlying that the process is physical adsorption and the regeneration can be achieved at low energy consumption. Furthermore, the gas uptake at 273 K is obviously higher than that at 298 K. It is reported that the exothermic process of CO_2 adsorption and lower temperature is favorable for CO_2 molecules adsorbing on surface of solid materials [35]. The maximum CO_2 adsorption capacity of SR-KOH and SS-KOH at 273 K is 4.09 mmol g^{-1} and 4.08 mmol g^{-1}. Under the same condition, SS-1000 with the least surface areas displayed the highest CO_2 adsorption capacity both at 273 K (4.52 mmol g^{-1}) and 298 K (3.08 mmol g^{-1}) (Table S2). To clarify this, the isosteric heat of adsorption value (Q_{st}) of CO_2 for the carbon samples was calculated using the CO_2 adsorption isotherms measured at 273 K and 298 K (Fig. S3), based on the Clausius-Clapeyron equation [36]. The Q_{st} can be used to determine the strength of interaction between the carbon materials and CO_2 molecules. The Q_{st} value of the three carbon samples varies in the range of 17–23 kJ mol^{-1} at low CO_2 uptake, corresponding to weak interactions with CO_2 and a relatively easy regeneration [36]. Among the three carbon materials, SS-1000 with the highest Q_{st} value corresponds a strong interaction between CO_2 molecules, resulting in the largest CO_2 adsorption capacity. The selectivity of CO_2/N_2 is calculated to be 40 from the initial slopes of the single component gas adsorption isotherms at 273 K (Fig. S4). It is well documented that the porous structure such as an abundance of micropores and suitable pore sizes of solid adsorbents is important in demining the CO_2 adsorption capacity [36,37]. From the PSD curves (Fig. 4b and c), SS-1000 possessed the highest micropore ratio (79%) and the narrowest PSD as well as the smallest pore size (0.46 nm, < 0.7 nm), which can strengthen the interaction between CO_2 molecules and pore walls, leading to increase in the adsorption capacity [36–38].

3.3. Iodine capture

Radioactive iodine isotopes including ^{129}I and ^{131}I are highly volatile contaminates that threatens environmental safety and human health. The concern of effective management for radioactive iodine and radiation protection reached the highest level after the nuclear accident at Fukushima in 2011 [6]. In this respect, several adsorbents were synthesized and used for iodine capture, such as zeolites, porous polymers, organic-organic hybrids and porous carbon materials, with the iodine loading varying from 125 wt% to 485 wt% (Table S3).

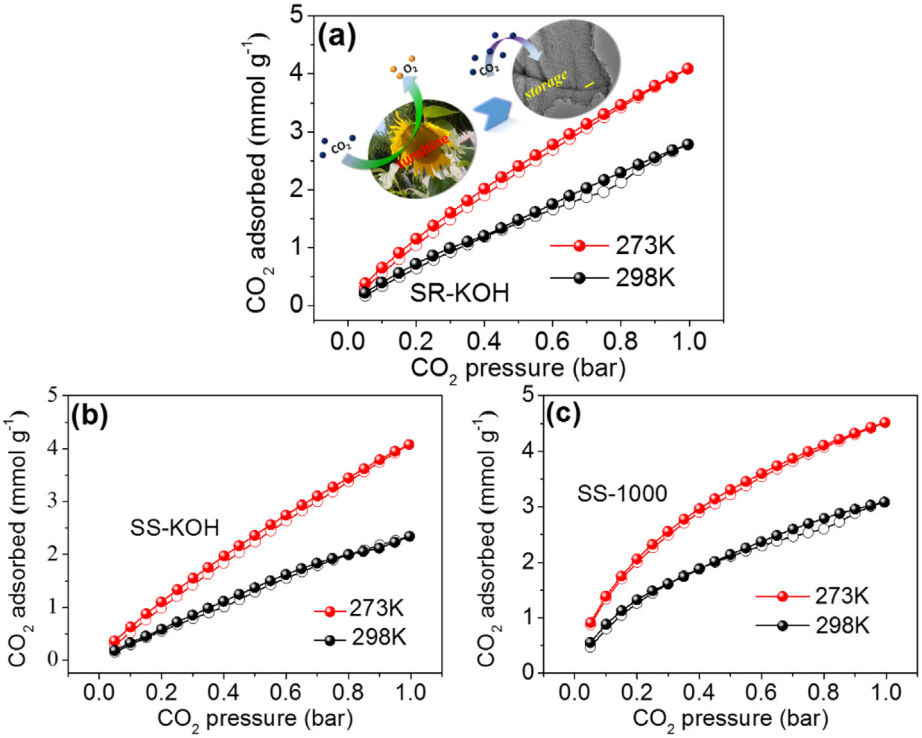

Fig. 5. CO_2 adsorption/desorption isotherms of (a) SR-KOH, (b) SS-KOH and (c) SS-1000 at different temperature. (a inset) Schematic illustration of CO_2 adsorption using the resulting porous carbons. TEM scale bar: 100 nm.

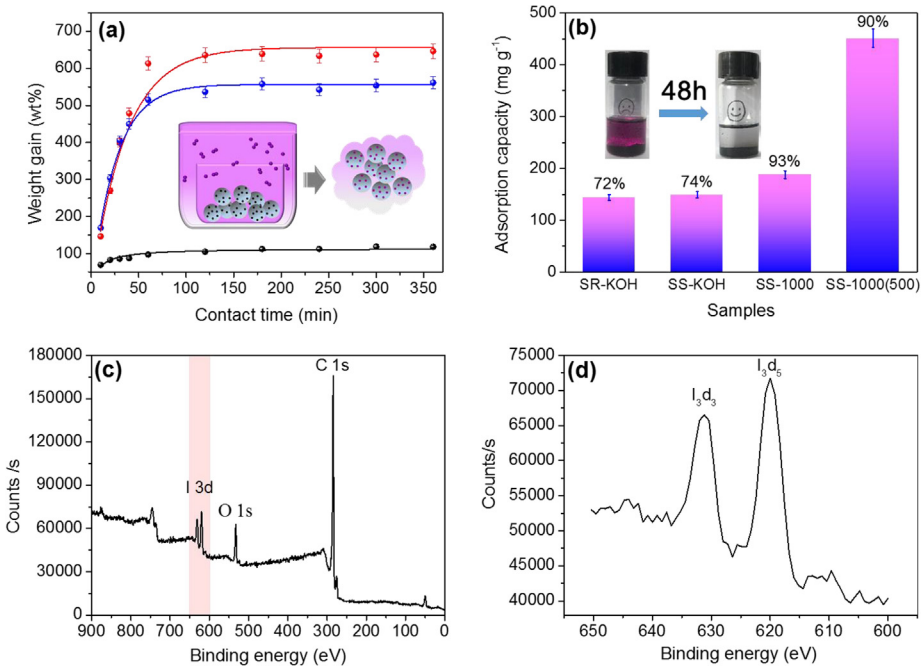

Fig. 6. (a) Gravimetric iodine uptake of carbon samples as a function of time at 350 K. Inset is the scheme of iodine adsorption experiment in solids. (b) The iodine adsorption by carbon samples in cyclohexane solutions with different concentration. Inset is the snapshot of SS-1000 in the iodine/cyclohexane solutions (200 mg L^{-1}) before and after adsorption. (c and d) XPS spectrum of SR-KOH after iodine adsorption.

Among these adsorbents, porous carbon materials are attracting considerable attention due to their chemical and thermal stability, environmental friendliness, low cost and abundant porosity as well as excellent absorbency, which promotes us to investigate the iodine adsorption capacity of the resulting carbon samples. The iodine loading amount was evaluated by gravimetric measurements at different time intervals by placing the carbon sample (taking SR-KOH as a model) and solid iodine in a sealed container at 350 K and ambient pressure (Fig. 6a inset, for details see Supporting Information), which is close to the actual nuclear-fuel reprocessing conditions. The iodine adsorption capacity was calculated based on mass grow of the measured sample (wt %) plotted as a function of contact time. The obtained kinetic curves are exhibited in Fig. 6a. From the curve, the iodine uptake for all carbon samples increases quickly and the equilibrium uptake for the carbon samples almost reached in 60 min. SR-KOH and SS-KOH exhibit iodine uptake of up to 646 wt% and 561 wt%, which considerably exceeds other porous solid materials (Table S3) [39–49]. The SS-1000 with the highest micropore ratio, which benefits to gas adsorption, however, the iodine loading amount for SS-1000 is far lower than that of SR-KOH and SS-KOH. As reported, the iodine uptake is strongly affected by the interaction between the adsorbents and iodine molecules at a low coverage. However, at a higher coverage, the surface areas and pore volumes of porous materials are crucial factor on the gaseous iodine uptake [50], which can be used to illustrate our case.

To further confirm it, XPS and FTIR was conducted to analyse the chemical structure of SR-KOH after iodine adsorption (named as SR-KOH@I_2). From the XPS spectrum (Fig. 6c and d), in addition to the peaks of C1s (285.0 eV) and O1s (532.6 eV), a double peak at 615–635 eV was observed, corresponding to I3d3 and I3d5 (Fig. 6c and d) and indicating that the valence of the trapped iodine is zero and the iodine in SR-KOH exists as I_2 [45]. The SR-KOH@I_2 exhibits a similar FTIR spectrum with SR-KOH and no obvious chemical bond interaction between iodine and SR-KOH was observed (Fig. 3b). Both the XPS and FTIR suggest that the gaseous iodine adsorption on SR-KOH dominates by the physical process. During the physical adsorption process, the porosity of the carbonaceous materials would supply an adequate void for iodine molecules and is an important factor on the adsorption capacity. As a result, a higher BET surface area of porous carbon is beneficial to the improvement on the gaseous iodine uptake [8].

The iodine capture capability of SR-KOH, SS-KOH and SS-1000 was further investigated in cyclohexane solution. As shown in Fig. 6b inset, the dark purple iodine/cyclohexane solution (5 mL) changes to almost colourless after SS-1000 (10 mg) adsorption for 48 h. The maximum iodine absorbency of SR-KOH, SS-KOH and SS-1000 in cyclohexane (200 mg l^{-1}) is 144 mg g^{-1}, 149 mg g^{-1} and 188 mg g^{-1}, corresponding to the removal efficiency of 72%, 74% and 93% (Fig. 6b). The SS-1000 exhibits an open and interpenetrating pore structure, which provides a channel and accelerates the transfer of iodine molecules in the liquid. As a result, the SS-1000 with the lowest BET surface area possess the highest iodine uptake in cyclohexane. The uptake reached up to 451 mg g^{-1} in the iodine/cyclohexane solution with a concentration of 500 mg g^{-1}, which is the highest value to our best knowledge [45]. According to the analysis on the sorption kinetic data (Fig. S5), the iodine sorption on SS-1000 fits well in pseudo-second-order kinetics model with a good linear correlation coefficient ($R^2 > 0.99$).

3.4. Removal of organic/oily contaminants from water

Owing to the increasing attention focused on the environmental pollution caused by oil spillages and the industrial discharge of organic solvents, there is a growing need to develop efficient absorbents to remove these oily and organic contaminants from water [51]. Porous carbons have been shown to be one of the most promising candidates for oil spill remediation from an economic view. However, the existence of oxygen-containing groups in these porous carbons make them adsorbing both water and oils/organics in a mixed aqueous phase, which hinders their adoption and absorption efficiency. In this regard, the porous carbons can be modified to obtain superhydrophobic surfaces, which has been proven a simple and efficient method to enhance affinity to oily/organic target compounds over water molecules. To obtain the superhydrophobic surfaces, we coated a thin polydimethylsiloxane (PDMS) coating over the entire surface of the porous carbons using a vapour deposition technique [51,52]. That is, the porous carbon (taking SS-1000 as a model) and a piece of PDMS film was placed into a sealed container and heated to 234 °C. Upon heat treatment, the Si-O bonds in PDMS chains would break and followed by the formation of a silicone coating on carbon particles owing to the cross-linking of the short PDMS chains (Fig. 7a). In the XPS spectrum of SS-1000@PDMS, an obvious peaks at 106.3 eV belong to the Si2p, corresponding to silicon

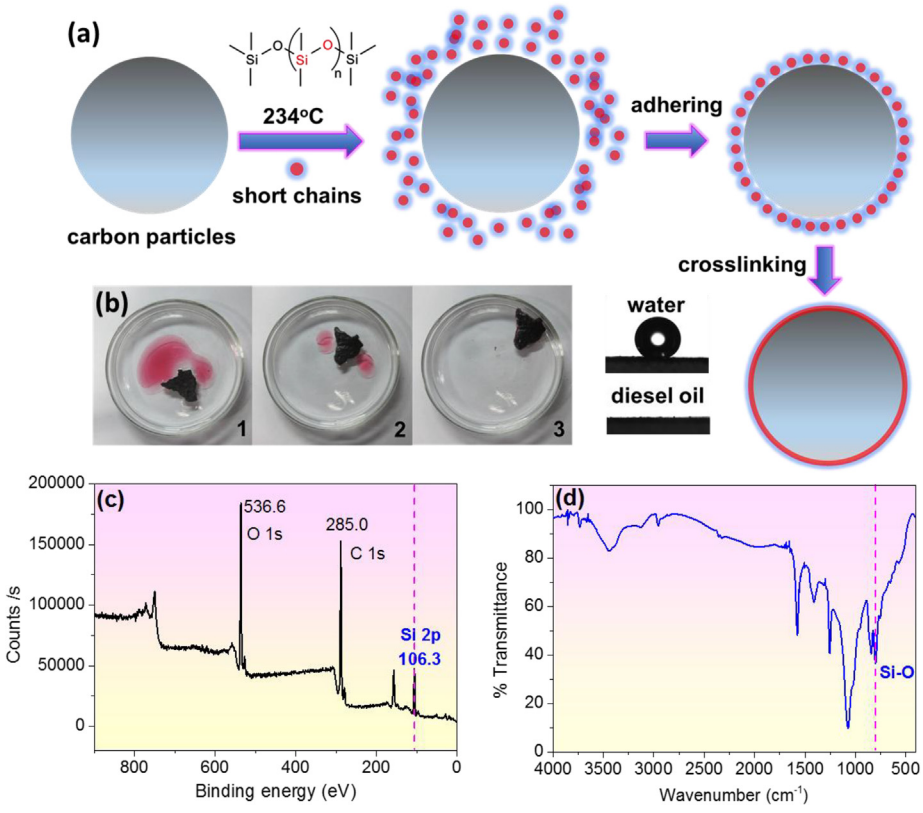

Fig. 7. (a) Formation mechanism of superhydrophobic carbon samples by PDMS modification. (b) Superhydrophobic SS-1000 for diesel oil (dyed with Red oil O)/water separation (left 1–3). Right is the water and diesel oil contact angle of SS-1000@PDMS. (c) XPS spectrum of SS-1000@PDMS. (d) FTIR spectrum of SS-1000@PDMS. (For interpretation of the references to color in this figure legend, the reader is referred to the web version of this article.)

content of ca. 21.5 at% (Fig. 7c). In the FTIR spectrum, a new absorption peaks near 800 cm^{-1} belong to the symmetrical stretching vibration of Si-O-Si (Fig. 7d). Both XPS and FTIR results verify the deposited of silicon moieties on the surface of SS-1000 after PDMS treatment. As a result, the silicon coating with low surface energy and the surface roughness of carbon particles were attributed to the improvement on the surface wettability. As anticipated, the PDMS modified SS-1000 (named as SS-1000@PDMS) becomes superhydrophobic with a water contact angle of 153.6° (Fig. 7b). Such superhydrophobic surface enable the benzene (dyed with Red oil O) in water selectively absorbed by SS-1000@PDMS in a few seconds without water uptake (Fig. 7b).

Taking advantages of the superhydrophobic and oleophylic property, these porous carbons could remove the oily/organic compounds from water with a high selectivity. The efficiency of absorption of these porous carbons can be referred to as weight gain using various organic solvents as the adsorbates (Fig. 8a). The adsorption capacities of SR-KOH@PDMS, SS-KOH@PDMS and SS-1000@PDMS for organics and oils with different polarity and density are 866–2795 wt%, 2027–5733 wt% and 752–1751 wt%, respectively, more higher than that of molecular sieves, activated carbon and attapulgite (< 1000 wt %). The recycling pollutants and the regeneration of porous carbons can be implemented using vacuum distillation after organics adsorption. As shown in Fig. 8b, the absorption ability of these porous carbons remained essentially identical even after 10 cycles of testing. Meanwhile, the water CA value was measured to 151° for SS-1000 after 10 adsorption/desorption cycles (Fig. 8b inset), suggesting excellent cyclic stability.

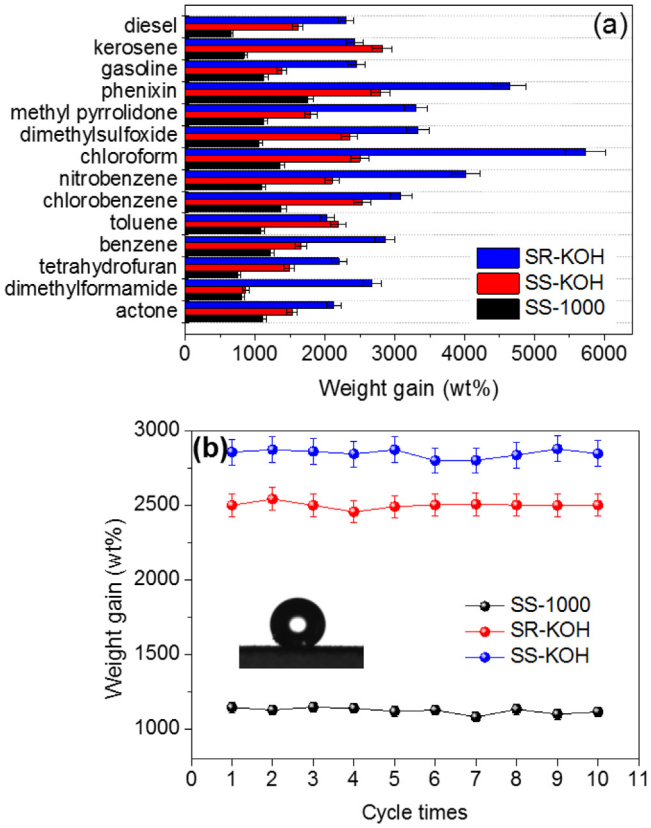

Fig. 8. (a) The adsorption capacity of carbon samples for various oils and organic solvents. (b) The changes in adsorption capacity of the carbon samples@PDMS after absorption cycles. Inset is the water CA measurement for SS-1000@PDMS after adsorption of gasoline for ten cycles.

4. Conclusion

Biomass-based porous carbons were synthesized from spongy flesh from receptacle and stalk of sunflowers using two methods-KOH activation and pyrolysis. The carbon samples (SR-KOH and SS-KOH) obtained from KOH activation are both composed with nano-sized carbon

particles and the pyrolysized sample (SS-1000) exhibits a connected flake morphology with film-liked exteriors. The BET surface areas of SR-KOH, SS-KOH and SS-1000 were calculated to 3072 m^2 g^{-1}, 2730 m^2 g^{-1} and 654 m^2 g^{-1}. Obviously, the treatment approach has an apparent effect on the morphology and porous texture. Encouraged by the excellent porous properties and unique structure, the resulting porous carbons can be used as functional sorbents for CO_2 storage, radioactive element and organic contaminates from water. It should be noted that the SR-KOH shows a high iodine affinity with an uptake of up to 646 wt%, which is the highest value reported to date. Considering their worldwide abundance and availability, the spongy flesh from receptacle and stalk of sunflowers could be act as a new biomass source of porous carbons, which may be provide a fundamental guidance for the practical application of biologically renewable resources from sunflowers.

Acknowledgements

The authors are grateful to the National Natural Science Foundation of China (Grant No. 51663012, 51462021), Support Program for Hongliu Young Teachers of LUT, Collaborative Innovation Team, Gansu Province, China (Grant No. 052005) and Innovation and Entrepreneurship Talent Project of Lanzhou (2017-RC-33).

Appendix A. Supplementary data

Supplementary data to this article can be found online at https://doi.org/10.1016/j.cej.2019.04.061.

References

[1] E.-J. Wang, Z.-Y. Sui, Y.-N. Sun, Z. Ma, B.-H. Han, Effect of porosity parameters and surface chemistry on carbon dioxide adsorption in sulfur-doped porous carbons, Langmuir 34 (2018) 6358–6366.
[2] G. Li, J. Sun, W. Hou, S. Jiang, Y. Huang, J. Geng, Three-dimensional porous carbon composites containing high sulfur nanoparticle content for high-performance lithium-sulfur batteries, Nat. Commun. 7 (2016) 10601.
[3] P. Mu, Z. Zhang, W. Bai, J. He, H. Sun, Z. Zhu, W. Liang, A. Li, Superwetting monolithic hollow-carbon-nanotubes aerogels with hierarchically nanoporous structure for efficient solar steam generation, Adv. Energy Mater. 8 (2018) 1802158.
[4] T. Jordan, Z.-L. Yu, S.-H. Yu, M. Antonietti, N. Fechler, Porous nitrogen-doped carbon monoliths derived from biopolymer-structured liquid precursors, Micropor. Mesopor. Mater. 255 (2018) 53–60.
[5] Y.J. Chen, S.F. Ji, Y.G. Wang, J.C. Dong, W.X. Chen, Z. Li, R.A. Shen, L.R. Zheng, Z.B. Zhuang, D.S. Wang, Y. Li, Isolated single iron atoms anchored on N-doped porous carbon as an efficient electrocatalyst for the oxygen reduction reaction, Angew. Chem., Int. Ed. 56 (2017) 6937–6941.
[6] H. Sun, P. La, Ruixia Yang, Zhaoqi Zhu, Weidong Liang, Baoping Yanga, An Li, Weiqiao Deng, Innovative nanoporous carbons with ultrahigh uptakes for captureand reversible storage of CO_2 and volatile iodine, J. Hazard. Mater. 321 (2017) 210–217.
[7] J. He, J.W.F. To, P.C. Psarras, H. Yan, T. Atkinson, R.T. Holmes, D. Nordlund, Z. Bao, J. Wilcox, Tunable polyaniline-based porous carbon with ultrahigh surface area for CO_2 capture at elevated pressure, Adv. Energy Mater. 6 (2016) 1502491.
[8] Z.-Y. Wu, C. Li, H.-W. Liang, Y.-N. Zhang, X. Wang, J.-F. Chen, S.-H. Yu, Carbon nanofiber aerogels for emergent cleanup of oil spillage and chemical leakage under harsh conditions, Sci. Rep. 4 (2014) 4079.
[9] Y. Wang, J. Wang, C. Ma, W. Qiao, L. Ling, Fabrication of hierarchical carbon nanosheet-based networks for physical and chemical adsorption of CO_2, J. Colloid Interf. Sci. 6 (2018) 1502491.
[10] Z. Xiao, Z. Yang, H. Nie, Y. Lu, K. Yang, S. Huang, Porous carbon nanotubes etched by water steam for high-rate large-capacity lithium-sulfur batteries, J. Mater. Chem. A 2 (2014) 8683–8689.
[11] H. Wang, Q. Gao, J. Hu, High hydrogen storage capacity of porous carbons prepared by using activated carbon, J. Am. Chem. Soc. 131 (2009) 7016–7022.
[12] J. Romanos, M. Beckner, T. Rash, L. Firlej, B. Kuchta, P. Yu, G. Suppes, C. Wexler, P. Pfeifer, Nanospace engineering of KOH activated carbon, Nanotechnology 23 (2012) 015401.
[13] M. Li, C. Liu, H. Cao, H. Zhao, Y. Zhang, Z. Fan, KOH self-templating synthesis of three-dimensional hierarchical porous carbon materials for high performance supercapacitors, J. Mater. Chem. A 2 (2014) 14844–14851.
[14] J. Gong, H. Lin, M. Antonietti, J. Yuan, Nitrogen-doped porous carbon nanosheets derived from poly(ionic liquid): hierarchical pore structures for efficient CO_2 capture and dye removal, J. Mater. Chem. A 4 (2016) 7313–7321.
[15] D. Chen, C. Chen, W. Shen, H. Quan, S. Chen, S. Xie, X. Luo, L. Guo, MOF-derived magnetic porous carbon-based sorbent: synthesis, characterization, and adsorption behavior of organic micropollutants, Adv. Powder Technol. 28 (2017) 1769–1779.
[16] S. Gupta, N.-H. Tai, Carbon materials as oil sorbents: a review on the synthesis and performance, J. Mater. Chem. A 4 (2016) 1550–1565.
[17] R. Wang, P. Wang, X. Yan, J. Lang, C. Peng, Q. Xue, Promising porous carbon derived from celtuce leaves with outstanding supercapacitance and CO_2 capture performance, ACS Appl. Mater. Interfaces 4 (2012) 5800–5806.
[18] Y. Feng, S. Liu, G. Liu, J. Yao, Facile and fast removal of oil through porous carbon spheres derived from the fruit of Liquidambar formosana, Chemosphere 170 (2017) 68–74.
[19] Y. Liang, C. Yang, H. Dong, W. Li, H. Hu, Y. Xiao, M. Zheng, Y. Liu, Facile synthesis of highly porous carbon from rice husk, ACS Sustainable Chem. Eng. 5 (2017) 7111–7117.
[20] H. Peng, J. Zhang, J. Zhang, F. Zhong, P. Wu, K. Huang, J. Fan, F. Liu, Chitosan-derived mesoporous carbon with ultrahigh pore volume for amine impregnation and highly efficient CO_2 capture, Chem. Eng. J. 359 (2019) 1159–1165.
[21] K. Huang, F. Liu, J. Fan, S. Dai, Open and hierarchical carbon framework with ultralarge pore for efficiently capture of carbon dioxide, ACS Appl. Mater. Interfaces 10 (2018) 36961–36968.
[22] B. Hu, K. Wang, L. Wu, S.-H. Yu, M. Antonietti, M.-M. Titirici, Engineering carbon materials from the hydrothermal carbonization process of biomass, Adv. Mater. 22 (2010) 1–16.
[23] X. Wang, S. Yun, W. Fang, C. Zhang, X. Liang, Z. Lei, Z.-H. Liu, Layer-stacking activated carbon derived from sunflower stalk as electrode materials for high-performance supercapacitors, ACS Sustainable Chem. Eng. 6 (2018) 11397–11407.
[24] B. Xu, H. Duan, M. Chu, G. Cao, Y. Yang, Facile synthesis of nitrogen-doped porous carbon for supercapacitors, J. Mater. Chem. A 1 (2013) 4565–4570.
[25] P. Mu, W. Bai, Z. Zhang, J. He, H. Sun, Z. Zhu, W. Liang, A. Li, Robust aerogels based on conjugated microporous polymer nanotubes with exceptional mechanical strength for efficient solar steam generation, J. Mater. Chem. A 6 (2018) 18183–18190.
[26] P. Mu, H. Sun, Z. Zhu, J. He, W. Liang, A. Li, Monolithic nanofoam based on conjugated microporous polymer nanotubes with ultrahigh mechanical strength and flexibility for energy storage, J. Mater. Chem. A 6 (2018) 11676–11681.
[27] F. Wang, F. Ren, D. Ma, P. Mu, H. Wei, C. Xiao, Z. Zhu, H. Sun, W. Liang, J. Chen, L. Chen, A. Li, Particle and nanofiber shaped conjugated microporous polymers bearing hydantoinsubstitution with high antibacterial activity for water cleanness, J. Mater. Chem. A 6 (2018) 266–274.
[28] M. Choi, R. Ryoo, Mesoporous carbons with KOH activated framework and their hydrogen adsorption, J. Mater. Chem. 17 (2007) 4204–4209.
[29] X. Wang, S. Yun, W. Fang, C. Zhang, X. Liang, Z. Lei, Z. Liu, Understanding chemical reactions between carbons and NaOH and KOH An insight into the chemical activation mechanism, Carbon 41 (2003) 267–275.
[30] R. Dawson, E. St€ockel, J.R. Holst, D.J. Adams, A.I. Cooper, Microporous organic polymers for carbon dioxide capture, Energy Environ. Sci. 4 (2011) 4239–4245.
[31] K. Wang, H. Huang, D. Liu, C. Wang, J. Li, C. Zhong, Covalent triazine-based frameworks with ultramicropores and high nitrogen contents for highly selective CO_2 capture, Environ. Sci. Technol. 50 (2016) 4869–4876.
[32] H. Wang, Z. Cheng, Y. Liao, J. Li, J. Weber, A. Thomas, C.F.J. Faul, Conjugated microporous polycarbazole networks as precursors for nitrogen-enriched microporous carbons for CO_2 storage and electrochemical capacitors, Chem. Mater. 29 (2017) 4885–4893.
[33] Z. Gao, Y. Zhang, N. Song, X. Li, Biomass-derived renewable carbon materials for electrochemical energy storage, ACS Appl. Mater. Interfaces 4 (2012) 5800–5806.
[34] Y. Li, G. Ruan, A.S. Jalilov, Y.R. Tarkunde, H. Fei, J.M. Tour, Biochar as a renewable source for high-performance CO_2 sorbent, Carbon 107 (2016) 344–351.
[35] S. Ghosh, M. Sevilla, A.B. Fuertes, E. Andreoli, J. Ho, A.R. Barron, Defining a performance map of porous carbon sorbents for highpressure carbon dioxide uptake and carbon dioxide-methane selectivity, J. Mater. Chem. A 4 (2016) 1–12.
[36] D. Qian, C. Lei, E. Wang, W. Li, A. Lu, A method for creating microporous carbon materials with excellent CO_2-adsorption capacity and selectivity, Chem. Sus. Chem. 7 (2014) 291–298.
[37] Y. Zhang, B. Li, K. Williams, W.-Y. Gao, S. Ma, A new microporous carbon material synthesized via thermolysis of a porous aromatic framework embedded with an extra carbon source for low-pressure CO_2 uptake, Chem. Commun. 49 (2013) 10269–10271.
[38] P. Nugent, Y. Belmabkhout, S.D. Burd, A.J. Cairns, R. Luebke, K. Forrest, T. Pham, S. Ma, B. Space, L. Wojtas, M. Eddaoudi, M.J. Zaworotko, Porous materials with optimal adsorption thermodynamics and kinetics for CO_2 separation, Nature 495 (2013) 80–84.
[39] D.F. Sava, M.A. Rodriguez, K.W. Chapman, P.J. Chupas, J.A. Greathouse, P.S. Crozier, T.M. Nenoff, Capture of volatile iodine, a gaseous fission product, by zeolitic imidazolate framework-8, J. Am. Chem. Soc. 133 (2011) 12398–12401.
[40] Y. Liao, Z. Cheng, W. Zuo, A. Thomas, C.F.J. Faul, Nitrogen-rich conjugated microporous polymers: facile synthesis, efficient gas storage, and heterogeneous catalysis, ACS Appl. Mater. Interfaces 9 (2017) 38390–38400.
[41] X. Qian, B. Wang, Z.-Q. Zhu, H.-X. Sun, F. Ren, P. Mu, C. Ma, W.-D. Liang, A. Li, Novel N-rich porous organic polymers with extremely high uptake for capture and reversible storage of volatile iodine, J. Hazard. Mater. 338 (2017) 224–232.
[42] M. Janeta, W. Bury, S. Szafert, Porous Silsesquioxane imine frameworks as highly effcient adsorbents for cooperative iodine capture, ACS Appl. Mater. Interfaces 10 (2018) 19964–19973.
[43] Z. Yan, Y. Yuan, Y. Tian, D. Zhang, G. Zhu, Highly efficient enrichment of volatile iodine by charged porous aromatic frameworks with three sorption sites, Angew Chem. Int. Ed. 54 (2015) 12733–12737.
[44] Y. Zhu, Y.-J. Ji, D.-G. Wang, Y. Zhang, H. Tang, X.-R. Jia, M. Song, G. Yu, G.-

C. Kuang, BODIPY-based conjugated porous polymers for highly efficient volatile iodine capture, J. Mater. Chem. A 5 (2017) 6622–6629.
[45] H. Li, X. Ding, B.-H. Han, Porous Azo-bridged porphyrin-phthalocyanine network with high iodine capture capability, Chem. Eur. J. 22 (11863–11868) (2016) 19964–19973.
[46] X. Qian, Z.-Q. Zhu, H.-X. Sun, F. Ren, A. Li, Capture and reversible storage of volatile iodine by novel conjugated microporous polymers containing thiophene units, ACS Appl. Mater. Interfaces 8 (2016) 21063–21069.
[47] F. Ren, Z. Zhu, X. Qian, W. Liang, P. Mu, H. Sun, J. Liu, A. Li, Novel thiophene-bearing conjugated microporous polymer honeycomb-like porous spheres with ultrahigh iodine uptake, Chem. Commun. 52 (2016) 9797–9800.
[48] Y. Liao, J. Weber, B.M. Mills, Z. Ren, C.F.J. Faul, Highly efficient and reversible iodine capture in hexaphenylbenzene-based conjugated microporous polymers, Macromolecules 49 (2016) 6322–6333.
[49] Q. Jiang, H. Huang, Y. Tang, Y. Zhang, C. Zhong, Highly porous covalent triazine frameworks for reversible iodine capture and efficient removal of dye, Ind. Eng. Chem. Res. 57 (2018) 15114–15121.
[50] D. Chen, Y. Fu, W. Yu, G. Yu, C. Pan, Versatile adamantane-based porous polymers with enhanced microporosity for efficient CO_2 capture and iodine removal, Chem. Eng. J. 334 (2018) 900–906.
[51] J. Yuan, X. Liu, O. Akbulut, J. Hu, S.L. Suib, J. Kong, F. Stellacci, Superwetting nanowire membranes for selective absorption, Nat. Nanotech. 3 (2008) 332–336.
[52] H. Sun, A. Li, Z. Zhu, W. Liang, X. Zhao, P. La, W. Deng, Superhydrophobic activated carbon-coated sponges for separation and absorption, Chem. Sus. Chem. 6 (2013) 1057–1062.